

Quantum path-integral study of the phase diagram and isotope effects of neon

R. Ramírez and C. P. Herrero

Instituto de Ciencia de Materiales de Madrid (ICMM),

Consejo Superior de Investigaciones Científicas (CSIC), Campus de Cantoblanco, 28049 Madrid, Spain

The phase diagram of natural neon has been calculated for temperatures in the range 17-50 K and pressures between 10^{-2} and 2×10^3 bar. The phase coexistence between solid, liquid, and gas phases has been determined by the calculation of the separate free energy of each phase as a function of temperature. Thus, for a given pressure, the coexistence temperature was obtained by the condition of equal free energy of coexisting phases. The free energy was calculated by using non-equilibrium techniques such as adiabatic switching and reversible scaling. The phase diagram obtained by classical Monte Carlo simulations has been compared to that obtained by quantum path-integral simulations. Quantum effects related to the finite mass of neon cause that coexistence lines are shifted towards lower temperatures when compared to the classical limit. The shift found in the triple point amounts to 1.5 K, i.e., about 6% of the triple-point temperature. The triple-point isotope effect has been determined for ^{20}Ne , ^{21}Ne , ^{22}Ne , and natural neon. The simulation data show satisfactory agreement to previous experimental results, that report a shift of about 0.15 K between triple-point temperatures of ^{20}Ne and ^{22}Ne . The vapor-pressure isotope effect has been calculated for both solid and liquid phases at triple-point conditions. The quantum simulations predict that this isotope effect is larger in the solid than in the liquid phase, and the calculated values show nearly quantitative agreement to available experimental data.

PACS numbers: 05.70.Fh, 05.30.-d, 05.70.Ce

I. INTRODUCTION

The electronic structure of atoms and molecules, encountered either in gas or condensed phases, is, within the framework established by the Born-Oppenheimer (BO) approximation, independent of the nuclear mass. Thus the BO potential energy surface (PES), that represents the energy landscape for the motion of the nuclei, results to be *independent* of the isotope mass. Many processes and properties depend on the movement of the atoms on the PES. Then, isotope effects may exist because the *kinetic energy* of the nuclei is mass dependent according to the laws of quantum mechanics. Thus, although potential energy parameters are isotope independent, the kinetic energy parameters are not.¹ Phase coexistence is an equilibrium property that depends on the kinetic energy of the atoms (think of a liquid in equilibrium with its vapor). Hence, the phase diagram of a given substance should depend on its nuclear mass and then display an isotope effect. We stress that this behavior is strictly of quantum mechanical nature, i.e., the classical limit in statistical thermodynamics *incorrectly* predicts that phase coexistence is a mass independent property. This erroneous prediction can be considered as a consequence of the *equipartition theorem* for the kinetic energy, that establishes that in the classical limit this energy is only a function of temperature and is therefore independent of the atomic mass.

The properties of rare-gas solids or fluids usually change as a function of the atomic mass in a systematic fashion, that has been used to study effects of the zero-point energy and isotope mass. There have been many studies of quantum effects in the phase coexistence of neon, which were initially motivated by the observation

that neon deviates from the principle of corresponding states, that is however rather accurately followed by argon, krypton, and xenon.² The calculation of *quantum corrections* to the classical limit of the phase diagram of neon is thus interesting because allows us to quantify systematic errors of treating the neon atoms as particles moving classically in the PES. However, we stress that these quantum corrections do not represent any kind of measurable property, i.e., they can not be directly compared to experimental data, because there is no way to perform measurements of the phase behavior in the classical limit. In this respect, the calculation of isotope effects in the phase diagram of neon results specially interesting because they can be directly compared to experimental data, offering then a direct test of the capability of the theoretical approach. Neon has three stable isotopes (^{20}Ne , ^{21}Ne , and ^{22}Ne) and the experimental study of isotope effects in its phase diagram is historically interesting. The observation by Keesom and Dijk³ in 1931 that ^{20}Ne was more volatile than ^{22}Ne at temperatures just above the triple point was the first demonstration of an isotope effect on the physical or chemical properties of matter, and this experiment was considered to be a proof of the existence of the zero-point energy.¹ An accurate determination of the vapor pressure difference between natural neon and pure ^{20}Ne and ^{22}Ne isotopes has been made by Bigeleisen and Roth⁴ and Furokawa.⁵ The vapor pressure isotope effect (VPIE) amounts to about 5% of the equilibrium pressure, being slightly larger for solid than for liquid phases. The triple-point isotope effect (TPIE) has been also measured for the ^{20}Ne and ^{22}Ne isotopes,⁶ and amounts to a temperature shift of 0.15 K. This difference might seem small, but it is relevant for thermometry as the triple point of natural neon ($T_p = 24.553$ K) is used

as fixed-point temperature standard in the International Temperature Scale of 1990 (ITS-90), and any deviation of the isotopic composition of natural neon leads to ambiguity in the reference temperature.⁷

The most employed quantum approaches to the phase diagram of neon are based either on perturbational methods using the Wigner-Kirkwood expansion of the quantum partition function in powers of \hbar , or on computer simulations using the path integral (PI) formulation of statistical mechanics. We are not aware of PI simulations of isotopic effects in the phase coexistence of neon. However, PI MC simulations of isotope effects in the lattice parameter and heat capacity of solid neon have been reported,⁸ showing good agreement to experimental data. The VPIE of liquid neon has been recently studied⁹ using a classical integral equation theory in order to obtain the parameters required for the statistical theory of isotope effects developed by Bigeleisen in 1961.¹⁰ The isotopic shift in the helium melting curve has been studied by PI MC simulations at temperatures where nuclear exchange effects associated to the nuclear quantum statistics are negligible.^{11,12} Isotope effects in the solid-liquid coexistence of Lennard-Jones (LJ) solids have been studied by the method of generating Landau free energy curves. This method was applied to study the melting curves of solid H₂ and D₂, for which quantum effects are expected to be much larger than for neon, due to its lighter molecular mass. At about 12 MPa the calculated melting temperature of *ortho*-D₂ and *para*-H₂ was of 22.3 and 18 K, respectively.¹³

In a summary of theoretical calculations of quantum corrections in neon, we should mention the study by Hansen and Weis¹⁴ of the coexistence curve of neon by a Wigner-Kirkwood expansion to order \hbar^2 . They found a lowering of the triple-point temperature of about 1.4 K and of the critical temperature of about 1.8 K due to quantum corrections. The quantum effect at the liquid-gas critical point was studied by Young by the Feynman-Hibbs effective potential method.¹⁵ An interesting prediction was that quantum effects modify the critical pressure, volume, and temperature, but no effect was predicted on the critical exponents. The neon liquid-vapor interface at the experimental triple point was studied by PI Monte Carlo (MC) simulations and compared to classical simulations, showing that the quantum interface is approximately one quarter of interatomic spacing wider than the classical counterpart.¹⁶ The liquid-vapor equilibrium of neon has been studied by Gibbs ensemble MC calculations by both the PI formulation,¹⁷ and a Wigner-Kirkwood expansion.¹⁸ Quantum effects in the liquid-vapor equilibrium were shown to be important and more significant in the liquid state. The critical temperature in the quantum simulation was found about 8% lower than in the classical limit.¹⁷ This value results to be larger than that of 4% predicted by a Wigner-Kirkwood expansion in Ref. [14]. The solid-liquid coexistence line of neon has been studied using a Wigner-Kirkwood effective potential at pressures between 10² and 4 × 10³ MPa,

showing that quantum effects are negligible in this range of pressures.¹⁹ A recent PI MC simulation has shown that at ambient pressure the melting temperature of neon is lowered by about 6 % (i.e. 1.5 K) when quantum effects are included.²⁰

In the present work we study the phase diagram of natural neon for temperatures in the range 17-50 K and pressures between 10⁻² and 2 × 10³ bar by calculation of the phase coexistence between solid, liquid, and gas phases. Moreover the VPIE of solid and liquid phases at triple-point conditions and the TPIE of ²⁰Ne and ²²Ne are also calculated and compared to experimental data. All results are obtained by PI MC simulations. Phase coexistence is obtained by requiring equality of the Gibbs free energy, G , of the phases in equilibrium. The calculation of G is performed using the Adiabatic Switching (AS)²¹ and Reversible Scaling (RS)²² approaches that are based on algorithms where the Hamiltonian (or a state variable as the pressure or inverse temperature) changes along the simulation run. The capability of both AS and RS methods to calculate free energies in the context of PI simulations has been recently analyzed in the study of neon melting,²⁰ and we will make extensive use of these free energy techniques in the present investigation. The influence of quantum effects in the phase diagram of neon will be quantified by comparing the predicted phase diagram calculated with and without atomic quantum effects included. The interatomic interaction between Ne atoms will be described by a Lennard-Jones pair potential, in analogy to our previous studies.^{8,20,23,24} We recognize that a better option for the neon pair potential is given by the fit to ab initio electronic structure calculations,^{18,25,26} however we have chosen the simple LJ pair potential for several reasons: the phase diagram in the classical case can be checked against a large number of previous LJ simulations,²⁷⁻²⁹ quantum effects in the three coexistence lines (solid-gas, solid-liquid, and liquid-gas) has not yet been calculated by PI simulations using the same LJ potential parameters, and the isotope effects in the phase diagram depend more on the kinetic energy than on the potential energy parameters.

The structure of this paper is as follows. In Sec. II we present the computational conditions employed in the PI simulations and the technique used to evaluate the free energy as a function of the isotope mass. The results obtained by PI and classical simulations for the three coexistence lines of neon are presented in Sec. III. The phase diagram of neon is displayed both in the pressure-volume ($P - V$) and in the density-temperature ($\rho - T$) domains. The TPIE of ²⁰Ne and ²²Ne is calculated and compared to experimental data in Sec. IV, while the VPIE of both solid and liquid phases of neon are derived in Sec. V, including also the comparison to experiment. Finally, we summarize our conclusions in Sec. VI.

II. METHODOLOGY

A. Computational conditions

In the PI formulation of statistical mechanics the partition function is calculated through a discretization of the integral representing the density matrix. This discretization serves to define cyclic paths composed by a finite number L of steps, that in the numerical simulation translates into the appearance of L replicas (or beads) of each quantum particle. Then, the implementation of PI simulations relies on an isomorphism between the quantum system and a classical one, derived from the former by replacing each quantum particle (here, atomic nucleus) by a ring polymer of L classical particles, connected by harmonic springs with a temperature- and mass-dependent force constant. Details on this computational method are given elsewhere.³⁰⁻³³ In this work the technical implementation of the PI simulations in the NPT and NVT ensembles (N being the number of particles) is identical to that presented in Ref. [20].

For the PI simulation of the phase diagram of natural neon, the rare gas atoms were treated as particles of mass $m_0 = 20.18$ amu interacting through a LJ potential with parameters $\epsilon = 3.2135$ meV and $\sigma = 2.782$ Å. The value of the parameter ϵ differs from that employed in our study of the melting transition of neon at ambient pressure,²⁰ where we found that the classical melting temperature ($T_{m,cl} = 24.95$ K) was closer to the experimental data ($T_m = 24.55$ K) than the quantum result ($T_{m,q} = 23.43$ K). Note that the classical melting temperature, $T_{m,cl}$, is proportional to the value of ϵ , and a significant deviation of $T_{m,q}$ from this proportionality is not expected in the quantum case. Thus, the parameter ϵ used in Ref. [20] has been increased by a scaling factor of $\alpha = 1.042$, which is roughly the factor needed to match experimental and calculated $T_{m,q}$ temperatures. The LJ potential was truncated for distances larger than $r_c = 4\sigma$ and shifted to zero to perform the MC sampling. The internal energy was corrected by adding back this potential shift in order to approximate the properties of the full LJ potential.

PI MC simulations were performed on cubic cells containing 500 atoms, assuming periodic boundary conditions. For the liquid, standard long-range corrections were computed assuming that the pair correlation function is unity, $g(r) = 1$ for $r > r_c$, leading to well-known corrections for the pressure and internal energies.³⁴ In the solid, the long range correction was a static-lattice approximation (called LR-s in Ref. [20]), that implies that atoms beyond a certain number of neighbor shells are arranged as in the perfect crystal ordering. From the value of the cutoff radius, we determine that the first twelve neighbor shells (representing 248 neighbors of a central atom) were dynamically included in the simulation. This approximation leads also to simple long-range corrections for the pressure and internal energies.^{35,36} The virial estimator was used for the calculation of the kinetic energy.³⁷

Solid phase simulations were started with the atoms on their ideal face-centered-cubic (fcc) positions, while the liquid and gas phase simulations were initialized by using random positions. The number of beads was set as $L = 15$, which has been shown to be adequate for the temperatures and pressures employed in this study.^{8,23,24} Typical runs consisted of 3×10^4 MC steps (MCS) for equilibration, followed by at least 10^5 MCS for the calculation of equilibrium properties. Some simulations were performed with larger runs up to 6×10^5 MCS, to check the convergence of the results. Classical results were obtained by setting the number of beads $L=1$ in our PI MC codes.

B. Free energy calculations

The thermodynamic integration (TI) is a standard technique that allows us to obtain the free energy of a system by the calculation of the reversible work needed to change the original system into a reference state of known free energy.³⁸⁻⁴⁰ The AS method is an alternative to the standard TI, where the reversible work is obtained by slowly changing the system Hamiltonian along the simulation run.²¹ RS is an efficient technique to obtain the free energy as a function of a state variable, typically T or P .²² The reversible work is calculated here, in way similar to the AS method, by slowly changing the state variable along the simulation run. The PI implementation of both AS and RS methods has been recently described in the study of solid-liquid coexistence of neon at ambient pressure and will not be repeated here.²⁰ An additional free energy method employed in this work is the Morales and Singer (MS) approach, that allows us to obtain the free energy difference between a quantum system and its corresponding classical limit in either the NVT or NPT ensembles.^{20,41} Here we merely summarize how these methods fit into our calculation procedure of the phase coexistence of neon.

The first step is to obtain the free energy of each phase (solid, liquid, or gas) at some appropriate reference point in the (T, P) plane. An NPT simulation of each phase at the chosen reference point is run to determine its equilibrium volume. In the case of the solid, the Helmholtz free energy, F , is then calculated by an AS simulation in the NVT ensemble, using the Einstein crystal as a reference. For the quantum case the reference is a quantum Einstein crystal,²⁰ while in the classical limit a classical Einstein crystal is used as reference.⁴²

In the case of a quantum fluid (either liquid or gas), the free-energy difference between the quantum and classical fluid is calculated with the MS approach in either the NVT or NPT ensembles.^{20,41} The excess free energy of the classical fluid is then obtained from the Johnson *et al.* parameterization.³⁴ Finally, the ideal gas contribution is added to obtain the total free energy of the quantum fluid.²⁰

In the case of the solid and liquid phases a finite size

correction was applied to the free energy F_N obtained for $N=500$ atoms by using the following relation

$$F = F_N - \alpha \frac{a(T)}{N}, \quad (1)$$

where F represents the infinite-size free energy, $a(T)$ is a constant that depends linearly on temperature (see Ref. [20]) and the scaling factor $\alpha = 1.042$ takes into account the change in the ϵ parameter employed in this work and in Ref. [20]. The value of $a(T)$ for both solid and liquid phases of neon is obtained from Tab. II and Eq. (21) in Ref. [20].

The coexistence temperature between two phases is then calculated at a given pressure by a free energy approach, by which the free energy of both phases is calculated over an overlapping range of temperatures by the RS method. The coexistence temperature is then determined by the point where the Gibbs free energy of both phases is identical.

C. Free energy isotope effect

The isotope effect in the phase coexistence of a substance is determined by the free energy difference between isotopes. Given an isotope of mass m , and assuming that the Helmholtz free energy of the natural isotopic composition, $F(m_0)$, is known by any of the methods summarized in Sec. II B, then the unknown free energy, $F(m)$, can be calculated by the expression

$$F(m) = F(m_0) + \int_{m_0}^m \frac{\partial F(m')}{\partial m'} dm'. \quad (2)$$

By considering the following thermodynamic definition of the kinetic energy K ,

$$K(m') = -m' \frac{\partial F(m')}{\partial m'}, \quad (3)$$

we get

$$F(m) = F(m_0) - \int_{m_0}^m \frac{K(m')}{m'} dm'. \quad (4)$$

This expression shows that the kinetic energy is the magnitude that determines the free energy difference between two isotopes. The implementation of the last equation in our PI simulations has been done by the AS method.²¹ Thus, in a simulation run with a number M of MCS, the particle mass is changed uniformly from the initial value m_0 to the final value m . The actual value of the mass at the simulation step i is,

$$m_i = m_0 + (i - 1)\Delta m, \quad (5)$$

where $\Delta m = (m - m_0)/(M - 1)$. The free energy difference, $\Delta F = F(m) - F(m_0)$, is then obtained as

$$\Delta F = - \sum_{i=1}^M w_i \frac{K_v(m_i)}{m_i} \Delta m, \quad (6)$$

where $K_v(m_i)$ is the virial estimator of the kinetic energy at step i . w_i is an integration weight factor ($w_i = 1$ except for $i=1$ or $i = N$, where $w_i = 0.5$). A calculation of isotope effects on solubilities of hydrogen has been done by a Fourier PI relation equivalent to Eq. (4) by using TI.⁴³ In the case of the NPT ensemble the mass dependence of the Gibbs free energy can be derived from the following relation analogous to Eq. (4)

$$G(m) = G(m_0) - \int_{m_0}^m \frac{K(m')}{m'} dm'. \quad (7)$$

For the calculation of VPIE at a given temperature it is useful to determine the Gibbs free energy as a function of pressure, provided that an initial value, $G(P_0)$, is already known. We have employed the following equation

$$G(P) = G(P_0) + \int_{P_0}^P V dP', \quad (8)$$

where we have made use of the relation $V = \partial G / \partial P$. The calculation of the integral in the last equation is also done by the RS method, i.e., the pressure P' is uniformly changed between P_0 and P along the simulation run and the value of $G(P)$ is calculated “on the fly” by solving numerically the integral in Eq. (8) as the simulation proceeds.²²

III. PHASE DIAGRAM OF NEON

The phase coexistence of natural neon has been derived from PI MC simulations. We present the results obtained for the three coexistence lines (solid-liquid, solid-gas, and liquid-gas). The studied temperature range is between 17-50 K and pressures were varied between 10^{-2} and 2×10^3 bar. The quantum results are compared to the classical limit and to available experimental data.

A. Solid-liquid coexistence

The free energy of both solid and liquid phases of neon over an overlapping range of temperatures that encompasses the melting point is shown in Fig. 1 for $P=1$ bar. The classical melting point is found at 26.1 K. The main quantum effect in the free energy is a shift of the classical data towards higher values. As this energy shift results larger for the solid than for the liquid phase, the melting temperature is displaced downward by about 1.5 K. The

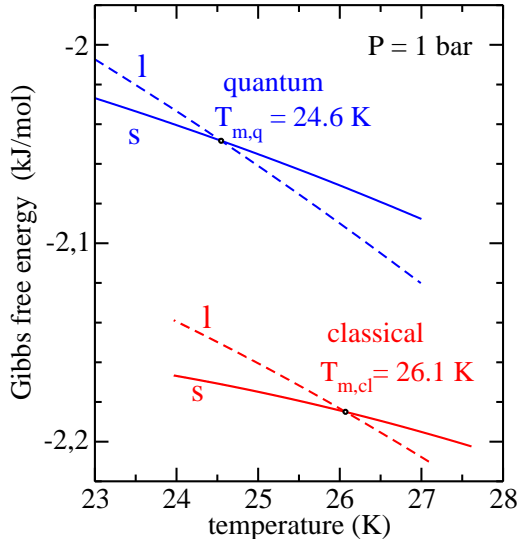


Figure 1: Melting temperature for fcc neon at 1 bar obtained by the condition of equal Gibbs free energy of the coexisting phases. Results are shown for both quantum and classical descriptions of solid (s) and liquid (l) phases.

slopes of the free energy curves are proportional to $-S$ (S being the entropy). From the figure, it is obvious that the entropy of the liquid phase is larger than that of the solid. Less obvious to the eye is that the entropy of both phases increases when quantum effects are included. At melting conditions ($P=1$ bar, $T_{m,cl} = 26.1$ K, and $T_{m,q} = 24.6$ K) the entropy of the solid phase amounts to 14.7 J/mol K (quantum) and 10.2 J/mol K (classical), while for the liquid phase the corresponding values are 27.7 J/mol K (quantum) and 23.8 J/mol K (classical). Therefore the consideration of quantum effects implies an increase of 44 % in the solid entropy and of 16 % in the liquid one.

The solid-liquid phase coexistence has been calculated for 9 different pressures up to 2 Kbar and the result for the melting line is shown in Fig. 2. We observe that the quantum melting line is displaced with respect to the classical limit. At zero pressure the quantum shift in the melting temperature, T_m , amounts to 1.6 K (about 6 % of T_m), while at 2 Kbar this shift is only of about 0.6 K (about 1 % of T_m). Therefore, the quantum effect in the melting temperature decreases as pressure goes up. This fact is in line with the Wigner-Kirkwood analysis of Ref. [19] for pressures between 10^3 and 2×10^4 bar. Our PI MC data show a reasonable overall agreement to experimental results.⁴⁴ The agreement is in part originated by our selection of the LJ parameter ϵ to fit the experimental melting temperature (24.55 K) at ambient pressure (see Subsec. II A). The broken line in the figure shows the classical simulation results of Ref. [27] for the LJ parameters employed here. These data are slightly shifted with respect to our classical melting line. We obtain somewhat higher melting temperatures for a given pressure. A possible reason for this discrepancy is that in both simulations the long range correction used for the

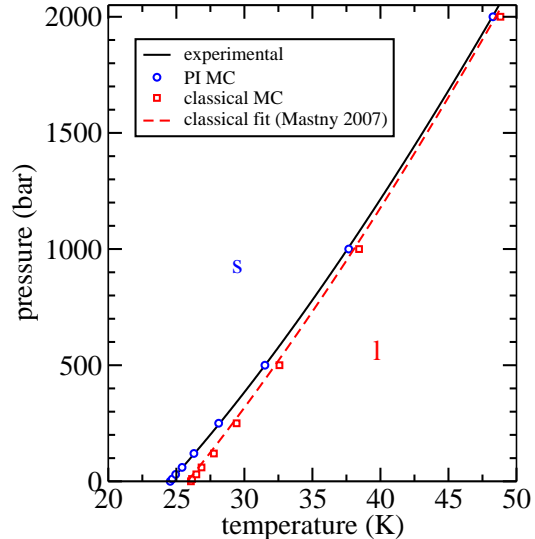


Figure 2: Solid-liquid (s-l) coexistence line of neon in the $P-T$ domain. The continuous line is the experimental result from Ref. [44]. Open circles and squares are the results of our PI MC and classical MC simulations, respectively. The broken line is the empirical fit to classical simulations given in Ref. [27].

solid phase and the LJ potential cutoff are different.

B. Solid-gas coexistence

The Gibbs free energy G of both solid and gas phases of neon is shown as a function of temperature in Fig. 3. The results derived for the gas from the Johnson parameterization are shown for five pressures between 10^{-2} and 0.5 bar. Neither quantum effects nor deviations from ideal behavior are significant in the displayed range of pressures for the gas free energies. The free energy of the solid corresponds to the data calculated at a pressure of 1 bar. At the scale of this figure, solid free energies at lower pressures are indistinguishable from the $P = 1$ bar data and are not represented (the PV term of the Gibbs free energy is of the order of 1 J/mol at these pressures). However, lower pressure results were calculated for the solid phase to determine the solid-gas coexistence line. In contrast to the gas behavior, quantum effects are important in the solid, and thus both classical and quantum free energy results are plotted in Fig. 3. It is interesting to note that at temperatures about 19 K the classical free energy of the solid displays a maximum, therefore below this temperature the entropy of the classical solid becomes negative and in fact it would tend to $-\infty$ as temperature goes down to zero. A simple way to derive this result is to work out analytically a harmonic model for the classical solid. This behavior of the classical entropy is known to be incompatible with the Nernst theorem that constitutes the third principle of thermodynamics.

The crossing points of the solid and gas free energy

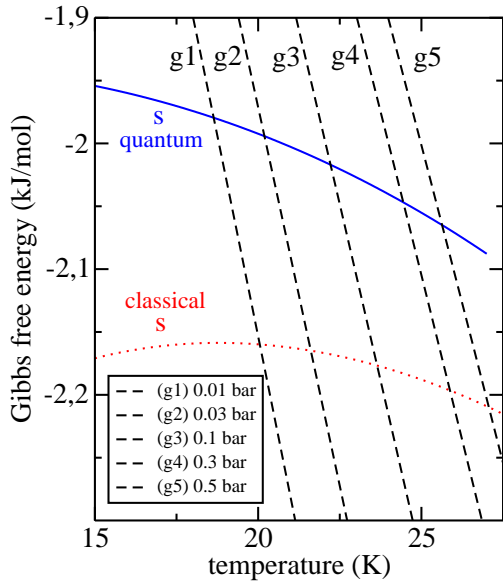


Figure 3: Gibbs free energies of the solid (s) and gas (g) phases of neon as a function of temperature. Gas results are shown for five different pressures. The free energy of the solid corresponds to a pressure of 1 bar. For the solid, the value of G for pressures between 0 and 1 bar are indistinguishable at the scale of the figure. Results for both quantum and classical simulations of solid fcc neon are shown.

curves, $G(T)$, at a given value of P determine the sublimation curve of the solid. We have calculated the solid-gas coexistence line at eighth values of P in the range between 10^{-2} and 0.8 bar. The results are shown in Fig. 4 and compared to available experimental data up to the triple-point temperature of neon.¹⁰ The PI MC results (open circles) display a constant shift of about 0.6 K with respect to the experimental data. We note that by the same scaling considerations as presented in Subsec. IIA for the LJ parameter ϵ , a decrease in the value of ϵ would produce a shift of our calculated solid-gas coexistence line toward lower temperatures. In this way we might improve the agreement of our sublimation line to experiment. However, the calculated melting line would then appear also shifted toward lower temperatures, and thus the good agreement to experimental data shown in Fig. 2 would be lost. We conclude that a simple LJ pair potential seems to be unable to describe both solid-gas and solid-liquid coexistence lines of neon in good agreement to experiment.

Our classical result for the sublimation line of neon is also given in Fig. 4. The shift with respect to the PI MC results is entirely due to quantum effects of the solid phase, as the gas behaves as an ideal gas for the displayed values of pressure and temperature. The broken line in the figure shows the fit of van der Hoef of the solid-gas coexistence using an empirical equation of state (EoS) for the LJ solid and the Johnson parameterization for the gas.⁴⁵ Our classical results are consistent with this fit.

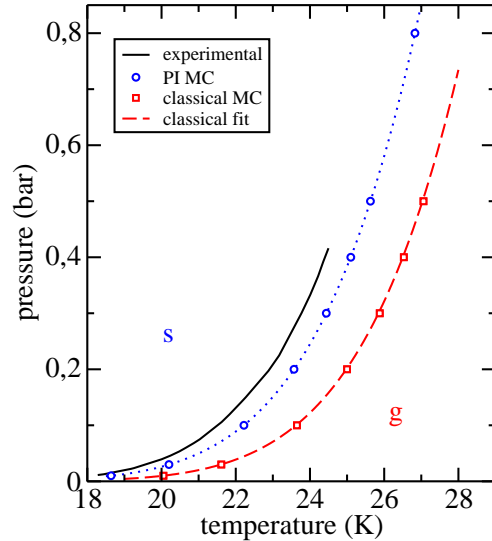


Figure 4: Solid-gas (s-g) coexistence curve of neon in the P - T domain. The continuous line is the experimental result from Ref. [10]. Open circles and squares are the results of our PI MC and classical MC simulations, respectively. The dotted line is a polynomial fit of fourth degree to the PI MC results. The broken line is a classical fit obtained by an empirical EoS in Ref. [45].

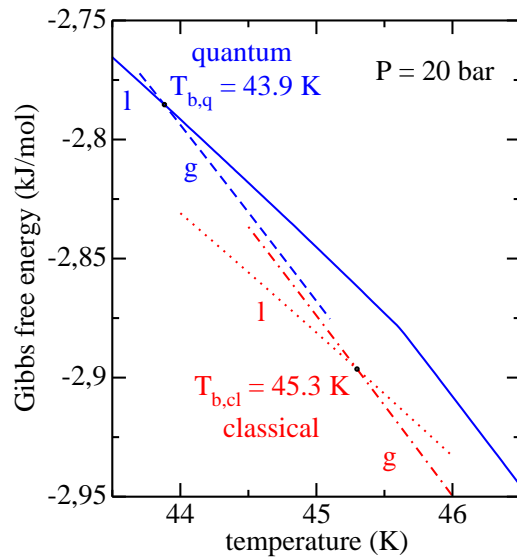


Figure 5: Determination of the boiling point, T_b , of neon at 20 bar. The calculated $G(T)$ curves for liquid (l) and gas (g) phases are displayed as a function of temperature. Results are displayed for both quantum and classical simulations.

C. Liquid-gas coexistence

The Gibbs free energy curves, $G(T)$, of liquid and gas neon phases at pressure of 20 bar are displayed in Fig. 5. At this pressure quantum corrections to the free energy of

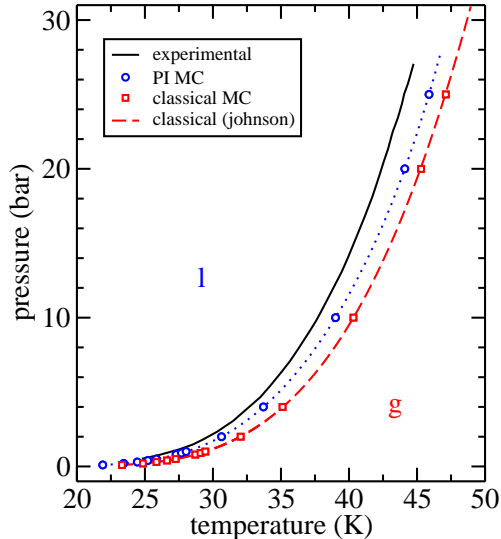


Figure 6: Liquid-gas (l-g) coexistence curve of natural neon in the $P-T$ domain. The continuous line is the experimental result from Ref. [46]. Open circles and squares are the results of our PI MC and classical MC simulations, respectively. The dotted line is a polynomial fit of sixth degree to the PI MC results. The broken line is the coexistence line obtained by using the parameterized EoS of Johnson.³⁴

the gas are significant, although smaller than in the case of the liquid phase. The shift in the boiling temperature due to quantum effects amounts to 1.4 K. The classical $G(T)$ curve for the gas phase was derived from the Johnson parameterization,³⁴ while for the liquid phase the classical curve was obtained by the RS method started at a temperature of $T = 44$ K. We have proceeded in this way to check the consistency of our classical MC liquid simulations against the Johnson EoS.³⁴

The liquid-gas coexistence line of natural neon is displayed in Fig. 6. Our classical results, derived from RS simulations of the free energy in the liquid phase, are consistent with the coexistence line directly obtained from the Johnson EoS.³⁴ The PI MC boiling line is shifted with respect to the classical result. Quantum corrections in the gas phase were found to be significant at pressures above 5 bar. Our quantum results deviate from the experimental boiling line.⁴⁶ Similar differences have been reported in Gibbs ensemble MC simulations of the vapor-liquid phase coexistence of neon,¹⁷ and the main reason for this discrepancy seems to be related to the necessity of including three body terms in the interaction potential.^{18,25,26}

We have performed NPT simulations of both liquid and vapor phases of neon at coexistence conditions to obtain the saturation densities. The critical temperature, T_c , has been then estimated by fitting the calculated densities of the liquid and vapor phases, ρ_l and ρ_g , to the scaling law⁴⁰

$$\rho_l - \rho_g = b(T_c - T)^\beta, \quad (9)$$

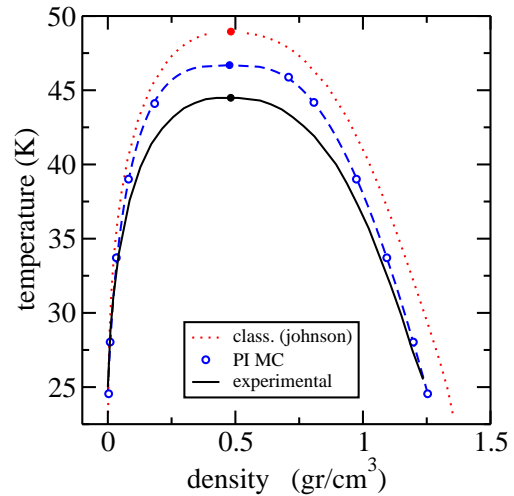


Figure 7: Density of coexistence of vapor and liquid phases. Experimental data are taken from Ref. [46], and classical results from Ref. [34]. The broken line is a fit of our PI MC results (open circles) to the scaling law presented in the text [Eqs. (9) and (10)]. Closed circles correspond to the critical point in the different approaches.

Table I: Comparison of the calculated critical point of neon with experimental data.

	experiment ^a	PI MC	classical ^b
T_c (K)	44.4	46.7	49.0
P_c (bar)	26.5	27.7	30.9
ρ_c (g/cm ³)	0.483	0.477	0.483

^aFrom Ref [46].

^bJohnson EoS,³⁴

where $\beta = 0.32$ is the non-classical critical exponent, which is expected to be valid also in the quantum case,¹⁵ and b is a constant. The values of T_c and b were obtained by a least-squares fit of our PI MC results. The critical density, ρ_c , was estimated by a fit to the law of rectilinear diameters,⁴⁰

$$\frac{1}{2}(\rho_l + \rho_g) = \rho_c + A(T - T_c). \quad (10)$$

where the constant A and the density, ρ_c , are the fitted parameters. The PI MC estimation of the critical pressure, P_c , was obtained from the fit of the boiling line in Fig. 6 at temperature T_c . The critical parameters estimated from our quantum simulations are compared to the experimental data and to the Johnson EoS in Tab. I, and the results for the saturation densities are presented in Fig. 7. The quantum correction to the saturation density is of opposite sign for vapor and liquid phases, while the vapor coexistence density increases, the liquid one decreases. Although the PI MC saturation densities are closer to experiment than the classical result, the deviation from experiment is notorious, especially as one approaches the critical point. This discrepancy is also found in previous simulations of the vapor-liquid coexistence of

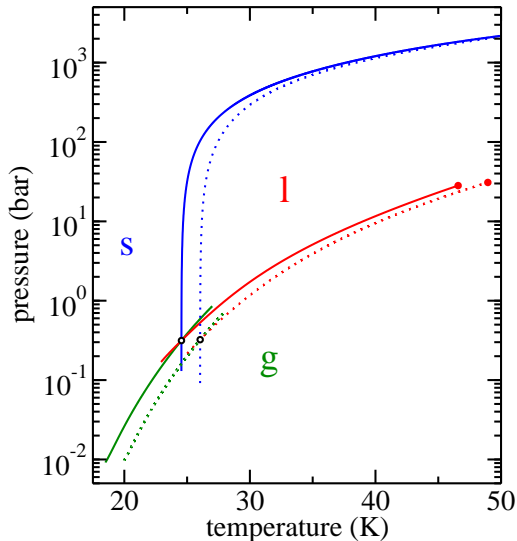


Figure 8: Phase diagram of natural neon in the pressure-temperature domain. Results are shown for the three coexistence lines between solid (s), liquid (l), and gas (g) phases. Continuous lines are derived from the PI MC results shown in Figs. 2, 4, and 6, while dotted lines are derived from the corresponding classical data in the same figures. Open circles represent the triple point and closed ones the critical point.

Table II: Comparison of predicted triple-point location of natural neon with experimental data.

	experiment	PI MC	classical
T_{tp} (K)	24.553 ^a	24.55	26.04
P_{tp} (bar)	0.433 ^a	0.315	0.323
$\rho_{tp,s}$ (g/cm ³)	1.424 ^b	1.429	1.494
$\rho_{tp,l}$ (g/cm ³)	1.247 ^b	1.254	1.313
$\rho_{tp,g}$ (g/cm ³)	-	0.0032	0.0031

^aRef. [5].

^bRef. [48].

neon using different pair potentials and quantum corrections, and reflects the importance of three body terms in the interaction potential to correctly describe phase coexistence near critical point conditions.^{17,18,26} From the difference between calculated and experimental values of T_c in Tab. I one can infer that near critical point conditions both quantum corrections and three body terms should be of similar importance.

D. P-T domain

The three calculated coexistence lines of natural neon are presented in Fig. 8 in the $P - T$ domain. Note that the pressure is plotted using a logarithmic scale. Continuous lines were derived from PI MC simulations, while dotted lines are classical results. The triple point is determined by the crossing of the three coexistence lines.

Table III: PI MC results for thermodynamic properties of natural neon at triple-point conditions.

	G (kJ/mol)	PV (kJ/mol)	U (kJ/mol)	S (J/mol K)
solid	-2.0492	0.0004	-1.6883	14.68
liquid	-2.0492	0.0005	-1.3719	27.57
gas	-2.0492	0.2002	0.2989	103.80

For both quantum and classical results we find that the three coexistence lines meet within a small temperature interval of 0.01 K and within a pressure interval of 0.002 bar. This small dispersion in the triple point determination is an internal check of the consistency of our results. Calculated triple-point properties are summarized in Tab. II. The value of T_{tp} predicted by the PI MC results is in good agreement to experiment, while classical simulations result in a higher value of T_{tp} by about 1.5 K. The equilibrium densities of the solid and liquid phases calculated by PI MC are also in good agreement to experiment. The calculated triple-point pressure, P_{tp} , is lower than the experimental data, and we do not observe any appreciable quantum correction to the value of P_{tp} . The calculated values of G , PV , internal energy (U), and S at triple-point conditions are summarized in Tab. III.

E. T- ρ domain

NPT simulations of coexisting phases have been performed along the three coexistence lines determined in the previous Subsections to obtain the phase diagram of natural neon in the temperature-density domain. The PI MC and classical results are presented in Fig. 9. The largest deviation between classical and quantum results is found for the solid phase, especially at temperatures below the triple point. We observe that quantum corrections to the liquid coexistence density at temperatures between the triple (T_{tp}) and critical points (T_c) results to be larger for the liquid-gas line than for the liquid-solid one. This behavior is probably related to the trend that quantum effects are comparatively less important as pressure increases.¹⁹ The liquid at temperatures between T_{tp} and T_c is under higher pressure if it is in equilibrium with the solid than if it is in equilibrium with its vapor (see the $P - T$ phase diagram in Fig. 8 and note that the coexistence pressure increases in both cases due to quantum effects).

IV. TRIPLE-POINT ISOTOPE EFFECT

We turn now to the study of the TPIE. We have previously obtained that the triple-point pressure, P_{tp} , of neon is nearly the same in both quantum and classical limits. Therefore one can reasonably assume that P_{tp} is nearly independent of the isotope mass. This fact sim-

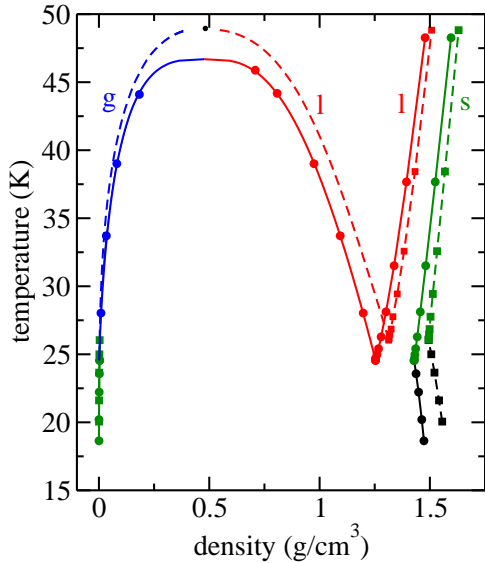


Figure 9: Phase diagram of natural neon in the temperature-density domain. Closed squares and circles are results obtained from classical MC and quantum PI MC simulations, respectively. Classical vapor and liquid densities were derived from the Johnson EoS,³⁴ while the continuous line through the quantum vapor and liquid densities is the fit to the scaling law presented in the text [Eqs. (9) and (10)]. Results are shown for the three coexistence lines between solid (s), liquid (l), and gas (g) phases.

Table IV: Free energy differences (ΔG_m , in J/mol) between neon isotopes and natural neon calculated at the triple point of natural neon. The calculated and experimental triple-point temperatures for each isotope are collected in the last lines.

	²⁰ Ne	²¹ Ne	²² Ne
ΔG_m (s)	3.8	-16.9	-36.4
ΔG_m (l)	3.6	-16.1	-34.8
T_{tp} (K) (PI MC)	24.538	24.608	24.673
T_{tp} (K) (exper.) ^a	24.540	-	24.687

^aRef. [5].

plifies the calculation of the TPIE that will be derived from a phase coexistence calculation at fixed pressure ($P_{tp} = 0.315$ bar). We have arbitrarily chosen to calculate the coexistence between solid and liquid phases, although any other two phases would be equally appropriate. The melting point of the neon isotopes will be determined by the same procedure shown in Fig. 1 for natural neon.

We take (T_{tp}, P_{tp}) of natural neon as reference point to calculate the Gibbs free energy of the solid and liquid phases of the neon isotope with mass m . The Gibbs free energy difference,

$$\Delta G_m = G(m) - G(m_0), \quad (11)$$

between the isotope of mass m and natural neon (m_0) is derived by an AS calculation using Eq. (7). The free

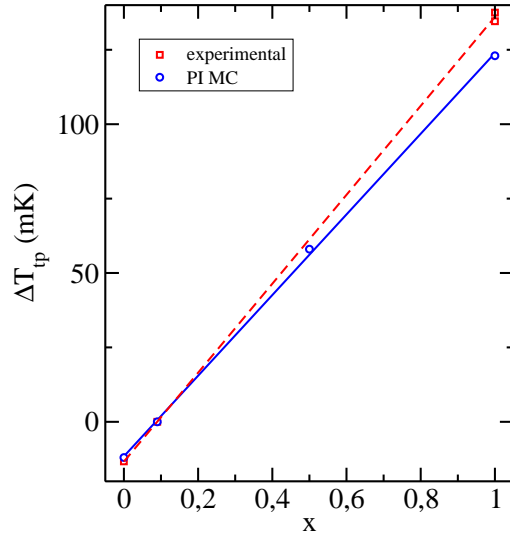


Figure 10: Triple-point temperature differences for the different neon isotopes as a function of the variable x defined in the text [Eq. (12)]. PI MC results are compared to experimental data.

energy $G(m_0)$ was given in Tab. III, and the results of ΔG_m for both solid and liquid phases are summarized in Tab. IV as a function of the isotope mass m . The triple-point temperatures, T_{tp} , obtained as the melting point of the isotopes at $P_{tp} = 0.315$ bar are also given in Tab. IV. The difference between the experimental triple-point temperatures of ²²Ne and ²⁰Ne is 0.147 K,⁵ while our PI MC simulations predict a value of 0.135 K. It is customary to represent the isotopic composition of a neon sample of mass m by a variable x , defined as

$$x = \frac{m - m_{20}}{2}, \quad (12)$$

where $m_{20} = 20$ amu. The PI MC results for the triple-point temperature difference with respect to natural neon are presented in Fig. 10 as a function of x . The calculated TPIE is compared to the experimental data taken from Ref. [7]. The linear behavior experimentally found as a function of x is reasonably reproduced by our simulations, however our slope is smaller than the experimental one.

V. VAPOR PRESSURE ISOTOPE EFFECT

The VPIE is experimentally tabulated as the logarithmic ratio of the isotopic vapor pressure, $\ln(p'/p)$, where p' and p are the vapor pressures of isotopes m and m' , with $m > m'$. We have calculated the VPIE for ²²Ne and ²⁰Ne at the critical points of both isotopes. First we consider the critical temperature of the lightest isotope, ²⁰Ne. Note that this temperature is lower than the triple-point temperature of ²²Ne. This implies that at this temperature the vapor of ²²Ne may coexist only with

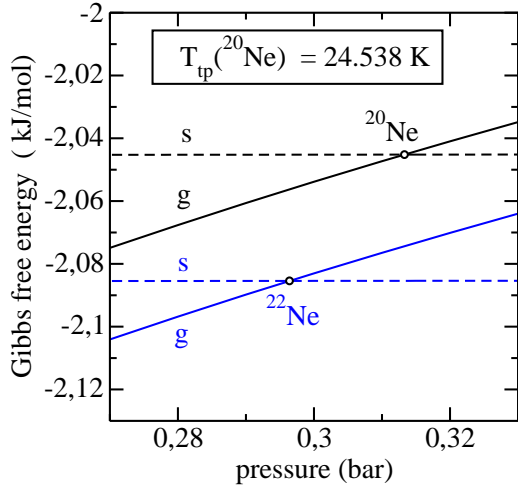


Figure 11: Determination of the vapor pressure of ^{20}Ne and ^{22}Ne at the triple point of ^{20}Ne by the study of the solid-gas coexistence.

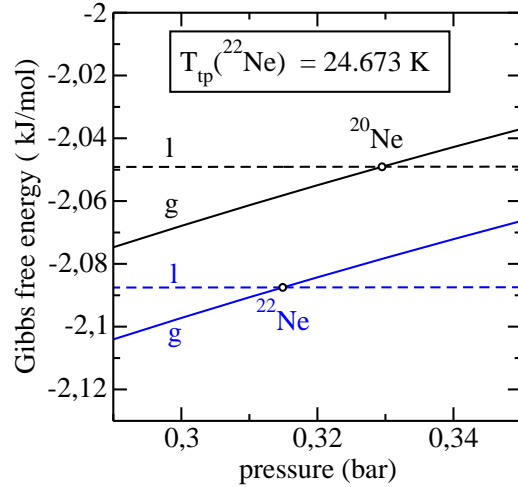


Figure 12: Determination of the vapor pressure of ^{20}Ne and ^{22}Ne at the triple point of ^{22}Ne by the study of the liquid-gas coexistence.

Table V: VPIE of ^{20}Ne and ^{22}Ne for solid (s) and liquid (l) phases at triple-point conditions. p' and p denote the vapor pressure of ^{20}Ne and ^{22}Ne , respectively.

	$\ln(p'/p)_s^a$	$\ln(p'/p)_l^b$
PI MC	0.056	0.047
exper. ^c	0.058	0.047

^aValues obtained at $T_{tp}(^{20}\text{Ne})$

^bValues obtained at $T_{tp}(^{22}\text{Ne})$

^cRef. [10]

its solid phase (as a visual help see the phase diagram in Fig. 8, where there appear two critical points at different temperatures). Therefore we have calculated the vapor pressure of ^{22}Ne and ^{20}Ne at $T_{tp}(^{20}\text{Ne})=24.538$ K by the study of the solid-gas coexistence. In Fig. 11 we have plotted the pressure dependence of the Gibbs free energy for both solid and gas phases of ^{22}Ne and ^{20}Ne . The free energy of the solid was calculated by a RS simulation using Eq. (8), while the free energy of the gas was obtained from the classical EoS.³⁴ The vapor pressures of ^{20}Ne , $p' = 0.313$ bar, and of ^{22}Ne , $p = 0.296$ bar, are read from the crossing points in the figure. The resulting value of $\ln(p'/p)$ is compared to available experimental data in Tab. V.¹⁰

The VPIE at the triple point temperature of the heavier isotope, ^{22}Ne , has been calculated by the study of the liquid-gas coexistence shown in Fig. 12. Gibbs free energies for the liquid phases were derived from PI MC simulations while the gas phase results correspond to the Johnson parameterization.³⁴ Here the vapor pressure of ^{20}Ne and ^{22}Ne are $p' = 0.330$ bar and $p = 0.315$ bar, and the calculated value of $\ln(p'/p)$ shows an excellent agreement to the experimental data (see Tab. V).^{10,47} Our simulations correctly reproduce that the VPIE is larger in the solid than in the liquid phase.

VI. CONCLUSIONS

The calculation of the phase diagram of neon by means of path integral simulations demonstrates that free energy techniques, previously used in classical simulations, can be also effectively employed to study quantum problems. In particular, we have made extensive use of the Adiabatic Switching²¹ and Reversible Scaling²² methods, that are based on algorithms where either the Hamiltonian, a state variable (pressure, temperature) or even an atomic mass are adiabatically changed along a simulation run. As long as this change is performed slowly (adiabatically), the associated reversible work is equal to the free energy difference between initial and final states. These free energy algorithms can be easily implemented in any code prepared for equilibrium simulations.

Our quantum simulations of the phase diagram of neon have focused on the study of two types of effects. The first one is a theoretical quantity not accessible by experimental measurements. This “quantum effect” is defined as the difference in phase coexistence properties obtained by applying either quantum or classical statistical mechanics. Such effects are not experimentally accessible, as there is no way to perform coexistence measurements of neon phases in the classical limit. Therefore, the calculation of these effects is interesting only if we want to quantify the errors of a classical treatment of phase coexistence. This interest exists because historically the approaches used to study phase coexistence of rare gas atoms were based on classical statistical mechanics. The second studied effect is real, in the sense that it can be experimentally measured. We refer here to isotope effects in the phase coexistence of neon, such as the triple-point temperature or vapor pressure. Classical statistical mechanics incorrectly predicts that phase coexistence is independent of the atomic mass, and therefore an isotope effect is classically forbidden.

We have found that quantum effects in the phase diagram of neon are significant at pressures below 2×10^3 bar. The whole solid-gas and liquid-gas coexistence lines are found below this limit. The main quantum effect found in the $P - V$ domain for these two lines is a shift of about 1.5 K toward lower temperatures. For the case of solid-liquid coexistence, a temperature shift is found that decreases with pressure, from a value of 1.5 K at triple point conditions to about 0.6 K at 2×10^3 bar. No significant quantum effects are found in the value of the triple-point pressure of neon.

The employed Lennard-Jones parameters have been able to reproduce reasonably the experimental melting line of neon in the studied pressure range up to 2×10^3 bar. However, the calculated solid-gas line shows a rigid shift of about 0.6 K toward higher temperatures when compared to experimental data. By decreasing the value of the Lennard-Jones parameter ϵ it is possible to shift the solid-gas line towards lower temperatures, but the solid-liquid line is shifted also by the same amount. Therefore it seems impossible to reproduce correctly both coexistence lines by employing a simple Lennard-Jones pair potential. The consideration of three body terms in the interaction potential is likely a necessary step to achieve better agreement to experiment. This consideration applies also for the liquid-gas coexistence, specially when approaching critical point conditions. The triple

point is reasonable reproduced by our quantum simulations, in particular the triple-point temperature and coexisting densities, while the predicted triple-point pressure is too low.

Our study of isotope effects in the triple-point temperature and vapor pressure of neon shows good agreement to experimental data. These isotope effects depend on the free energy difference between neon isotopes, that is a function of the kinetic energy and therefore not as dependent on the details of the interaction potential. The calculated difference between the triple-point temperatures of ^{22}Ne and ^{20}Ne was 0.135 K, while the experimental result is 0.147 K.⁵ Our quantum simulations correctly reproduce that ^{20}Ne is more volatile than ^{22}Ne and the calculated vapor-pressure isotope effect in both solid and liquid phases at triple point conditions show near quantitative agreement to experimental data.

Acknowledgments

This work was supported by Ministerio de Ciencia e Innovación (Spain) through Grant No. FIS2006-12117-C03 and by CAM through project S-0505/ESP/000237. The authors benefited from discussions with E. R. Hernández and A. Antonelli.

-
- ¹ G. Jancso and W. A. Van Hook, *Chem. Rev.* **74**, 689 (1974).
- ² E. A. Guggenheim, *J. Chem. Phys.* **13**, 253 (1945).
- ³ W. H. Keeswom and H. van Dijk, *Proc. Acad. Amsterdam* **34**, 42 (1931).
- ⁴ J. Bigeleisen and E. Roth, *J. Chem. Phys.* **35**, 68 (1961).
- ⁵ G. T. Furokawa, *Metrologia* **8**, 11 (1972).
- ⁶ K. Clusius, P. Flubacher, U. Piesbergen, K. Schleich, and A. Sperandio, *Z. Naturforsch.* **15**, 1 (1960).
- ⁷ F. Pavese, B. Fellmuth, K. D. Hill, D. Head, L. L. Y. Hermier, T. Nakano, A. Peruzzi, H. Sakurai, A. Szmyrka-Grzebyk, A. G. Steele, et al., *Int. J. Thermophys.* **29**, 57 (2008).
- ⁸ C. P. Herrero, *Phys. Rev. B* **65**, 014112 (2001).
- ⁹ J. N. C. Lopes, A. A. H. Pádua, L. P. N. Rebelo, and J. Bigeleisen, *J. Chem. Phys.* **118**, 5028 (2003).
- ¹⁰ J. Bigeleisen, *J. Chem. Phys.* **34**, 1485 (1961).
- ¹¹ J. L. Barrat, P. Loubeyre, and M. L. Klein, *J. Chem. Phys.* **90**, 5644 (1989).
- ¹² M. Boninsegni, C. Pierleoni, and D. M. Ceperley, *Phys. Rev. Lett.* **72**, 1854 (1994).
- ¹³ C. Chakravarty and R. M. Lynden-Bell, *J. Chem. Phys.* **113**, 9239 (2000).
- ¹⁴ J.-P. Hansen and J.-J. Weis, *Phys. Rev.* **188**, 314 (1969).
- ¹⁵ R. A. Young, *Phys. Rev. Lett.* **45**, 638 (1980).
- ¹⁶ J. Q. Broughton, F. F. Abraham, and J. A. Barker, *Phys. Rev. A* **40**, 924 (1989).
- ¹⁷ Q. Wang and J. K. Johnson, *Fluid Phase Equilib.* **132**, 93 (1997).
- ¹⁸ M. Venkatraj, C. Bratschi, H. Huber, Robert, and J. Gdanitz, *Fluid Phase Equilib.* **218**, 285 (2004).
- ¹⁹ J. Solca, A. J. Dyson, G. Steinebrunner, B. Kirchner, and H. Huber, *J. Chem. Phys.* **108**, 4107 (1998).
- ²⁰ R. Ramírez, C. P. Herrero, A. Antonelli, and E. R. Hernández, *J. Chem. Phys.* **129**, 064110 (2008).
- ²¹ M. Watanabe and W. P. Reinhardt, *Phys. Rev. Lett.* **65**, 3301 (1990).
- ²² M. de Koning, A. Antonelli, and S. Yip, *Phys. Rev. Lett.* **83**, 3973 (1999).
- ²³ C. P. Herrero and R. Ramírez, *Phys. Rev. B* **71**, 174111 (2005).
- ²⁴ R. Ramírez and C. P. Herrero, *Phys. Rev. B* **72**, 024303 (2005).
- ²⁵ P. S. Vogt, R. Liapine, B. Kirchner, A. J. Dyson, H. Huber, G. Marcelli, and R. J. Sadus, *Phys. Chem. Chem. Phys.* **3**, 1297 (2001).
- ²⁶ A. E. Nasrabad, R. Laghaei, and U. K. Deiters, *J. Chem. Phys.* **121**, 6423 (2004).
- ²⁷ E. A. Mastny and J. J. de Pablo, *J. Chem. Phys.* **127**, 104504 (2007).
- ²⁸ M. A. Barroso and A. L. Ferreira, *J. Chem. Phys.* **116**, 7145 (2002).
- ²⁹ R. Agrawal and D. A. Kofke, *Mol. Phys.* **85**, 43 (1995).
- ³⁰ R. P. Feynman, *Statistical Mechanics* (Addison-Wesley, New York, 1972).
- ³¹ M. J. Gillan, *Phil. Mag. A* **58**, 257 (1988).
- ³² D. M. Ceperley, *Rev. Mod. Phys.* **67**, 279 (1995).
- ³³ C. Chakravarty, *Int. Rev. Phys. Chem.* **16**, 421 (1997).
- ³⁴ J. K. Johnson, J. A. Zollweg, and K. E. Gubbins, *Mol. Phys.* **78**, 591 (1993).

- ³⁵ M. H. Müser, P. Nielaba, and K. Binder, *Phys. Rev. B* **51**, 2723 (1995).
- ³⁶ A. Cuccoli, A. Macchi, G. Pedrolli, V. Tognetti, and R. Vaia, *Phys. Rev. B* **56**, 51 (1997).
- ³⁷ M. F. Herman, E. J. Bruskin, and B. J. Berne, *J. Chem. Phys.* **76**, 5150 (1982).
- ³⁸ J. G. Kirkwood, *J. Chem. Phys.* **3**, 300 (1935).
- ³⁹ M. P. Allen and D. J. Tildesley, *Computer Simulation of Liquids* (Clarendon Press, Oxford, 1987).
- ⁴⁰ D. Frenkel and B. Smit, *Understanding Molecular Simulation* (Academic Press, San Diego, 1996).
- ⁴¹ J. J. Morales and K. Singer, *Mol. Phys.* **73**, 873 (1991).
- ⁴² J. M. Polson, E. Trizac, S. Pronk, and D. Frenkel, *J. Chem. Phys.* **112**, 5339 (2000).
- ⁴³ T. L. Beck, *J. Chem. Phys.* **96**, 7175 (1992).
- ⁴⁴ R. K. Crawford and W. B. Daniels, *J. Chem. Phys.* **55**, 5651 (1971).
- ⁴⁵ M. A. van der Hoef, *J. Chem. Phys.* **117**, 5092 (2002).
- ⁴⁶ V. A. Rabinovich, A. A. Vasserman, V. I. Nedostup, and L. S. Veksler, *Thermodynamic Properties of Neon, Argon, Krypton, and Xenon* (Springer-Verlag, Berlin, 1988).
- ⁴⁷ W. L. Tew, *Int. J. Thermophys.* **29**, 67 (2008).
- ⁴⁸ W. L. Vos, J. A. Schouten, D. A. Young, and M. Ross, *J. Chem. Phys.* **94**, 3835 (1991).